

## PROTECTIVE VACUUM-ARC COATINGS ON ZIRCONIUM ALLOY FUEL CLADDING TO PREVENT CATASTROPHIC ACCIDENTS AT NUCLEAR REACTORS

*A.S. Kuprin, V.A. Zuyok, V.A. Belous, V.D. Ovcharenko, E.N. Reshetnyak, R.L. Vasilenko, G.N. Tolmachova, Ya.O. Kushtym*  
*National Science Center “Kharkov Institute of Physics and Technology”, Kharkiv, Ukraine*  
*E-mail: kuprin@kipt.kharkov.ua*

The processes of vacuum arc deposition of multicomponent coatings based on Cr, Ti, Al, Fe, Y, Si, and their nitrides with a thickness of 5...9  $\mu\text{m}$  for the protection of zirconium alloy fuel rods were developed. The composition, structure, and mechanical properties of the coatings were determined by electron microscopy, energy dispersive X-ray spectroscopy, X-ray diffraction analysis, and nanoindentation. Comparative studies of the protective properties of coatings during high-temperature oxidation of Zr1Nb tubes were carried out. It was found that metal coatings with a high chromium content have excellent protective properties during tests under simulated accident conditions. They are simultaneously resistant to high-temperature corrosion in air at 750...1100 °C and in water steam during thermal cycling up to 1020 °C. Hard nitride coatings, which significantly strengthen the surface of the zirconium alloy and provide good protection against oxidation in air, are less effective in water steam under thermal cycling. The coatings and processes of synthesis developed at NSC KIPT can be useful for improving fuel cladding made of zirconium alloys of the world's leading nuclear fuel producer Westinghouse Electric Company.

### INTRODUCTION

Zirconium alloys are used as a base material of fuel claddings in the PWR and BWR-type nuclear reactors all over the world. The Zr-based alloys are widely applied due to their low thermal-neutron capture cross-section, good mechanical properties and high waterside corrosion resistance at normal operating temperature up to 350 °C. However, after severe nuclear accident at Fukushima NPP in Japan in 2011, the issue of fuel stability and reactor safety has attracted much attention in the world. As a result, the concept of accident tolerant fuel (ATF) has been developed with improved performance in normal operation and in accidents [1]. The aim of implementation of accident tolerant materials is to make the fuel and the cladding more robust and tolerant to sudden rise in the temperature to levels above 1000 °C. That is, the application of ATF materials will significantly reduce the risk of plant operation. The implementation of resilient materials will allow longer plant operation and extend the periods between refueling that will also decrease the cost of plant operation [2].

After near a decade of research, three main categories of accident tolerant materials for the cladding emerged (Coated zirconium alloys, Monolithic FeCrAl alloys, Silicon carbide composites) [3]. In particular, tests in various laboratory conditions show that the application of Cr coatings by Physical Vapor Deposition (PVD) on zirconium alloys traditionally used for fuel cladding proves to be a very effective and economical way to increase resistance, which has good potential for industrial application [4].

The world's leading nuclear fuel manufacturers, such as Westinghouse, Framatom and General Electric are intensively testing new fuel claddings in research and commercial reactors [5]. Westinghouse and Framatom [6] made the choice in favor of the Cr-coated zirconium

alloys and SiC composites, and General Electric in benefit of Cr-coated zirconium alloy and FeCrAl alloy cladding.

The Westinghouse Electric Sweden AB in an autoclave simulating both PWR and BWR water chemistries tested the corrosion protection properties of cathodic arc CrN and TiN coatings [7]. Schematic corrosion mechanisms for each material and environment are proposed. The Westinghouse focus was on Cr-coatings deposited with cold spray, which performed well in autoclave and under steam tested environments [8-10]. A passivating layer of chromia formed during autoclave exposure, and a protective scale of chromia prevented any oxidation of the Zr substrate for up to 40 min in 1200 °C steam. The formation of a Cr<sub>2</sub>Zr phase at the Cr/Zr interface was observed both under autoclave [8, 9] and under simulated accident conditions [10].

The use of nanocrystalline multi-component coatings based on transition metal nitrides, which are intensively developed and implemented to strengthen the surface of cutting tools and machine parts in various industries is of considerable interest for the protection of the zirconium alloys fuel claddings [11–13]. In particular, vacuum arc coatings based on TiN with the addition of Al, Cr, Si, Y not only have increased hardness, but also demonstrate high temperature and corrosion resistance [14–16]. In addition, the hard surface layer can protect the fuel element from scratches and damage during reloading, when it rubs against spacer grids and in other cases during normal reactor operation.

Comparison of the protective properties of Zircaloy samples with coatings of different compositions, such as Cr, CrN, CrAlN, TiAlN, TiN/TiAlN, Ti<sub>2</sub>AlC, Ti<sub>3</sub>SiC<sub>2</sub>, and CrAlC, showed that Cr and CrN are the most promising [17]. In an attempt to develop a nuclear fuel

cladding that is more tolerant to loss-of-coolant-accidents (LOCA), ceramic coatings (based on  $Ti_{1-x}Al_xN$  or TiN) were deposited onto a ZIRLO™ substrate by cathodic arc deposition [18–20].

Promising results are demonstrated by the technology of applying various types of single- and multi-layer vacuum-arc coatings based on metals, alloys, and metal nitrides to fuel claddings made of Zr1Nb alloy, developed at NSC KIPT [21–26]. The deposition of coatings is realized from the direct flow of metal plasma of the vacuum arc without its filtration, which is due to the need to simplify and reduce the cost of the process of depositing coatings on full-size tubes on an industrial scale.

Thus, the implementation of projects on the creation of ATF materials is a relevant, effective and important way of solving the problem of further development and increasing the safety of nuclear energy [27].

The aim of this work is to experimentally investigate the effectiveness of protection of fuel rod claddings made of Zr1Nb zirconium alloy by deposition vacuum arc coatings of various compositions based on Cr, Ti, Al, Fe, Y, Si, and their nitrides under model conditions of an accident in air and water steam.

## 1. MATERIAL AND METHODS

Cylindrical fragments of fuel cladding tubes with a diameter of 9.1 mm and a length of 10 mm made of Zr1Nb zirconium alloy and flat disks from the same alloy with a diameter of 10 mm for X-ray diffraction studies were used as samples.

The coatings based on multicomponent metallic (TiAlCrY, FeCrNi) and nitride (TiAlN, TiAlYN, TiAlSiN, TiAlCrYN) systems with a thickness of 5...9  $\mu\text{m}$  were deposited from unfiltered metal plasma at the Bulat-6 facility [28]. Two metal plasma sources were located coaxially at the ends of the cylindrical vacuum chamber, opposite each other at a distance of 300 mm from the substrate holder. A specially designed substrate holder with planetary rotation was used to ensure uniform coatings on all sides of the samples. Cathodes from chromium (99.9%), stainless steel Cr18Ni10T (SS), titanium alloys:  $Ti_{50}Al_{50}$ ,  $Ti_{49}Al_{50}Y_1$ ,  $Ti_{60}Al_{32}Si_8$ ,  $Ti_{47}Al_{50}Cr_2Y_1$  with a diameter of 60 mm were used to obtain the coatings.

The initial vacuum in the chamber was  $1 \cdot 10^{-3}$  Pa. Prior to deposition, the samples were bombarded with argon ( $Ar^+$ ) and chromium ions at an argon pressure of ~1 Pa and a negative bias voltage of 1200 V on the samples. A pulsed sputtering mode was used to keep the sample temperature below 500 °C. Nitrogen ( $P = 1.5 \dots 2$  Pa) was used as a reactive gas for obtaining nitride coatings, and metal coatings were deposited in a vacuum of at least  $2 \cdot 10^{-3}$  Pa. The arc discharge current for chromium and stainless steel cathodes was 90 A, and for titanium alloy cathodes 75 A. The bias potential on the samples during the deposition of metal coatings was -50 V, and nitride coatings -150 V. The metal coatings had a thin Cr sublayer, and the nitride coatings had a double Cr/CrN sublayer.

Investigations of the samples microstructure before and after oxidation were performed using scanning

electron microscope JEOL JSM-7001F. Chemical composition of the coatings was determined by energy dispersive X-ray spectroscopy – EDS.

The phase composition of the samples was studied by X-ray diffraction analysis using a DRON-3 diffractometer. Cu-K $\alpha$  radiation is used in all investigations. XRD measurements are conducted in Bragg–Brentano ( $\theta$ – $2\theta$ ) configuration in the range of angles from 20 to 90 degrees. The average crystallite size (coherent scattering zone) in the coatings was determined by the broadening of the diffraction lines using the Scherrer formula.

Hardness and Young's modulus of the coatings were studied by nanoindentation using a Nanoindenter G200 device with a continuous stiffness measurement (CSM) attachment [29].

The samples were tested for resistance to high-temperature air oxidation by annealing them in an ohmic heated furnace for 7200 s at 750 °C and for 3600 s at 1020 and 1100 °C. The tubes were placed in special alundum cuvettes, weighed with them, and then inserted into the furnace after reaching the required temperature. The heating rate of the samples was ~20 °C/s, and the cooling rate was -5 °C/s. Thermal cycling testing of samples in water steam was carried out at the “thermoshock” installation at temperatures from 20 to 1020 °C. Thermal cycling mode: heating from 20 °C to a temperature of 1020 °C for 100 s, holding for 20 min, cooling to 20 °C for 100 s. The number of cycles at each test temperature was 3. After the tests, the samples were weighed with and without alundum cuvettes to account for the mass of the deposited oxide film and photographed, and the studies were carried out on the grinds of the cross-sections of the tubes cut from the middle part of the samples before and after oxidation. The outer side of the tube was coated and the inner side was uncoated.

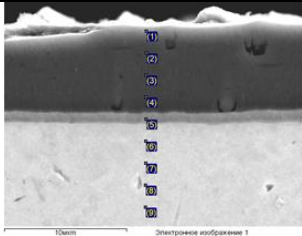
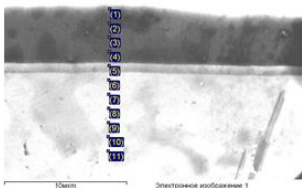
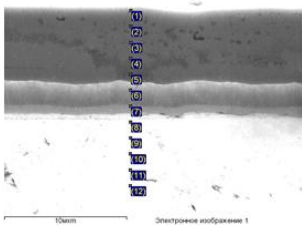
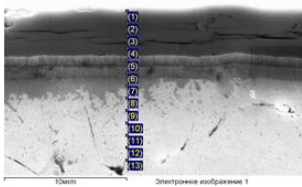
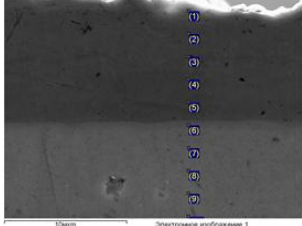
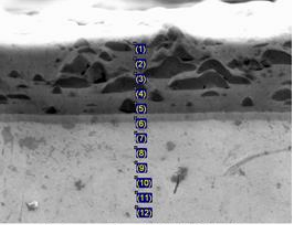
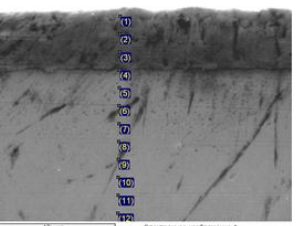
## 2. RESULTS AND DISCUSSION

The sequence of layers in the synthesized coatings, their thickness, surface elemental composition determined by EDS, and electron microscopic images of cross-sections are shown in Table 1. The electron microscopic images show that all coatings have a dense homogeneous structure of layers. The exception is the coating with a top layer of TiAlSiN, in which longitudinal cracks are observed. The formation of cracks is due to high internal stresses and mechanical impact during the grinding of the sample. A feature of the arc discharge is the presence in the plasma flow of drops of cathode material – macroparticles that, falling into the coating, can deteriorate its properties. It can be seen that the number, size, and distribution of droplets in the coatings vary depending on their composition, which is primarily related to the peculiarity of burning the cathode spots on a complex alloyed cathode in a vacuum and reaction gas ( $N_2$ )

In the coating with the top nitride layer of TiAlN, a small number of embedded droplets is visible. Addition of Y and Cr to the composition of TiAlN helps to reduce the number of droplets. However, in the case of the TiAlCrY metal layer, a large number of flattened and bound droplets are observed. The best quality in terms of the absence of cracks and inclusions are the metal layers of Cr and SS, as well as the sublayer of CrN.

Table 1

Composition, thickness, mechanical properties and electron microscopic images samples with coatings


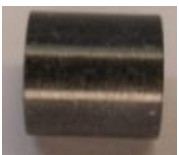



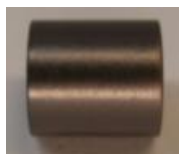
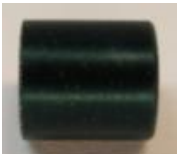
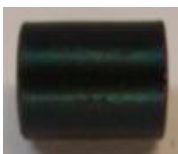


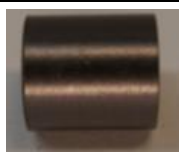

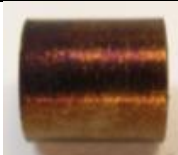


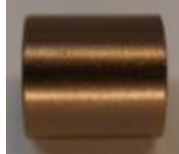
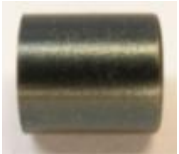



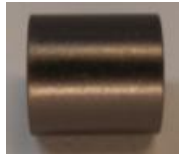
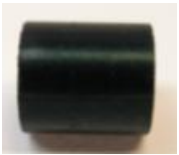



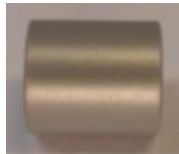














| Coating                  | Thickness of the layers, $\mu\text{m}$ | Composition of the top layer, at. %                                  | Hardness H, GPa | Young's modulus E, GPa | SEM images of the coatings structure  |
|--------------------------|--|--|-----------------|------------------------|---|
| Zr1Nb<br>without coating | –                                      | –  | 2,3             | 110                    | –   |
| Cr/CrN/TiAlN             | 0.1/0.3/6                              | Ti – 28<br>Al – 24<br>N – 48   | 32              | 341                    |    |
| Cr/CrN/TiAlYn            | 0.1/0.3/4.7                            | Ti -24<br>Al – 24.5<br>Y – 0.5<br>N – 51                             | 33              | 352                    |    |
| Cr/CrN/TiAlCrYn          | 0.1/1/6.4                              | Ti – 22<br>Al – 24<br>Cr – 3<br>Y – 0.6<br>N – 50.4                  | 35              | 360                    |   |
| Cr/CrN/TiAlSiN           | 0.3/1/4.7                              | Ti – 25.5<br>Al – 22<br>Si – 2.5<br>N – 50                           | 45              | 425                    |  |
| Cr/SS                    | 0,1/9                                  | Fe – 64<br>Cr – 33.3<br>Ni – 1.9<br>Mn – 0.4<br>Ti – 0.2<br>Si – 0.2 | 3               | 180                    |  |
| Cr/TiAlCrY               | 0.5/8                                  | Ti – 38.5<br>Cr – 32<br>Al – 19<br>Y – 0.5                           | 5               | 200                    |  |
| Cr                       | 9                                      | Cr - 99  | 4               | 300                    |  |

The analysis of the elemental composition of coatings shows that the ratio of components is slightly different compared to the composition of cathodes, especially for metal coatings, which may be due to selective sputtering of the growing surface during synthesis. For nitride coatings, a sufficiently good correspondence of the Ti/Al ratio with the cathode was obtained, and the Si content significantly decreases, which is typical for vacuum-arc coatings of such systems [14–16, 30, 31]. Nitrogen content in nitride coatings is up to 50 at.%.

Deposition of coatings should not reduce the physical and mechanical characteristics of fuel rods. Table 1 shows the results of measurements of the mechanical properties of the coatings by the nanoindentation method. As can be seen from the table, all coatings have higher hardness and Young's modulus compared to the Zr1Nb alloy, which is characterized by a hardness of 2.3 GPa. The hardness of metal coatings is 3...5 GPa, and the hardness of nitride coatings reaches 32...45 GPa.

Table 2

External image of the fuel claddings tubes fragments before and after high-temperature oxidation in air and steam

| Coating                     | Initial   | Air   |   |   | Steam   |
|-----------------------------|---|---|---|---|---|
|                             |   | 750 °C,<br>120 min  | 1020 °C,<br>60 min  | 1100 °C,<br>60 min  | 1020 °C<br>(3×20 min)   |
| Zr1Nb<br>without<br>coating |    |    |    |    |    |
| Cr/CrN/<br>TiAlN            |    |    |    |    |    |
| Cr/CrN/<br>TiAlYN           |  |  |  |  |  |
| Cr/CrN/<br>TiAlSiN          |  |  |  |  |  |
| Cr/CrN/<br>TiAlCrYN         |  |  |  |  |  |
| Cr/TiAlCrY                  |  |  |  |  |  |
| Cr/SS                       |  |  |  |  |  |
| Cr                          |  |  |  |  |  |

The external image of the samples from the sections of the fuel rods before and after the tests for high-temperature oxidation in air and water steam is shown in Table 2. At oxidation temperature of 750 °C (2 h) in air, all samples changed their color. No cracks or delamination in the samples were observed. After oxidation at a temperature of 1020 °C for an hour, cracks and traces of white oxide are visible in the gray oxide film on the uncoated Zr1Nb sample, while no shedding or cracks are observed on the coated samples. During the same oxidation time at 1100 °C, a white oxide with macro-cracks forms on the uncoated sample. White color and cracks appeared on the samples with Cr/CrN/TiAlN and Cr/CrN/TiAlSiN nitride coatings. On the samples with Cr/CrN/TiAlYn and Cr/CrN/TiAlCrYn nitride coatings, the color is dark and cracks are rare. On the samples with metal coatings Cr/SS, Cr/TiAlCrY and Cr, the surface color is dark and no cracks are visible.

In Fig. 1 shows weight gain histograms of the samples after testing for high-temperature oxidation. All coated samples oxidize in air significantly less than uncoated Zr1Nb samples at all test temperatures, and this advantage increases with increasing temperature. Metal coatings demonstrate the best resistance to high-temperature corrosion. Thus, the increase in weight of samples with Cr coating at 1100 °C is 6.3 times less than that of uncoated samples.

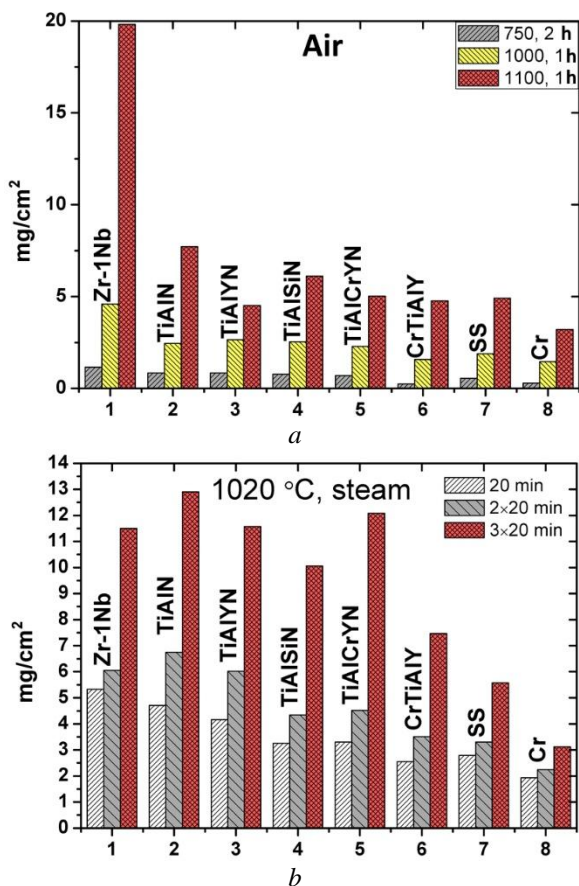


Fig. 1. Weight gain of samples after oxidation: in air at 750 (2 h), 1020 (1 h), 1100 °C (1 h) (a); after thermocycling (3 times for 20 min) in a steam at 1020 °C (b) (only the top layer of the coating is indicated)

This is despite the fact that the tube samples are coated only on the outside. Among the nitride coatings with the top layer of TiAlYn and TiAlCrYn have an advantage.

An even clearer picture of the effects of high-temperature corrosion is provided by SEM images of the samples cross-sections after testing, as shown in Table 3. After the tests, the coatings maintain good adhesion to the substrate. They do not delamination and have a homogeneous thickness. A dense oxide layer forms on an uncoated Zr1Nb sample at an oxidation temperature of 750 °C. With increasing temperature and thermal cycling cracks and pores appear in this layer. Sample begins to crumble, but despite this, has a mass increase (see Fig. 1) much greater than that of the coated samples, which indicates intensive oxidation. All coatings prevent destruction of the sample surface.

Table 4 shows the thickness of the oxidized layer into the samples after the tests, determined in their cross sections by the EDS method. During oxidation in air, the depth of oxygen penetration on all coated samples is significantly smaller than on the uncoated sample at all test temperatures of 750...1100 °C. Both metal and nitride coatings have better resistance to high-temperature oxidation in air than the Zr1Nb alloy. At an annealing temperature of 1100 °C, the uncoated sample is oxidized to a depth of 130 µm within an hour. In the Cr/CrN/TiAlN coated sample, oxygen penetrates only 12 µm, but still reaches the zirconium substrate. Addition of Y, Si, and Cr to TiAlN reduces the depth of the oxidized layer by 4 times, which is significantly less than the thickness of the coatings. However, a feature of nitride coatings is the possibility of cracks forming at the interface between the coating and the base, which leads to local oxidation to a depth of ~ 10 µm of samples with Cr/CrN/TiAlYn and Cr/CrN/TiAlSiN coatings. The Cr/CrN/TiAlCrYn coating has minor cracks but no focal oxidation. The formation of cracks can be caused by high compressive stresses and brittleness of hard coatings.

The thickness of oxygen penetration into metal coatings is 3...5 µm. For the Cr/SS coating, mutual diffusion of coating and substrate elements is observed in a layer with a thickness of ~ 3 µm. To prevent diffusion, it is advisable to increase the thickness of the Cr sublayer. The best coating in this test is Cr, which has no cracks and the thickness of the oxidized layer does not exceed 3 µm.

The structure of the zirconium alloy and coated samples before and after the tests was studied by X-ray structural analysis. First, it should be noted that the flat samples for X-ray studies were subjected only to high-temperature oxidation in air at 1100 °C, 60 min. X-ray diffraction patterns of the samples in the initial state and after oxidation are shown in Figs. 2–7.

The diffractogram of the Zr1Nb sample in the initial state (see Fig. 2,a) shows diffraction lines of a single phase, α-Zr, with a hexagonal close-packed (hcp) structure. During high temperature annealing in air, the surface of this sample is actively oxidized to form ZrO<sub>2</sub> oxide, which has a monoclinic crystal lattice (see Fig. 2,b). The diffractogram of the annealing Zr1Nb sample shows no lines of Zr or intermediate oxides with



a lower oxygen content, indicating that the surface is completely oxidized to  $ZrO_2$  to a depth of at least  $10\ \mu\text{m}$ .

Diffraction patterns of samples with nitride coatings are shown in Figs. 3–6. The diffraction patterns contain narrow lines of the  $\alpha$ -Zr substrate (marked with the letter S) and the CrN sublayer. Regardless of the elemental

composition, the only crystalline phase in the surface layer of the coatings is a solid solution based on cubic nitride with a crystal lattice of the NaCl type (structural type B1), which is characteristic of TiN. On the diffraction patterns, dashed lines show the positions of the diffraction lines of TiN with a crystal lattice period of  $0.424\ \text{nm}$ .

Table 3

Cross-section SEM images of the samples with coatings after high-temperature oxidation

| Coating               | Air              |                  |                  | Steam              |
|-----------------------|------------------|------------------|------------------|--------------------|
|                       | 750 °C (120 min) | 1020 °C (60 min) | 1100 °C (60 min) | 1020 °C (3×20 min) |
| Zr1Nb without coating |                  |                  |                  |                    |
| Cr/CrN/TiAlN          |                  |                  |                  |                    |
| Cr/CrN/TiAlYN         |                  |                  |                  |                    |
| Cr/CrN/TiAlSiN        |                  |                  |                  |                    |
| Cr/CrN/TiAlCrYN       |                  |                  |                  |                    |
| Cr/TiAlCrY            |                  |                  |                  |                    |
| Cr/SS                 |                  |                  |                  |                    |
| Cr                    |                  |                  |                  |                    |

Table 4

Thickness of the oxidized layer on samples with coatings (EDX analysis) after high-temperature oxidation

| Coating               | Thickness of the oxidized layer, $\mu\text{m}$ |                  |                  |                    |
|-----------------------|--|------------------|------------------|--------------------|
|                       | Air  |                  |                  | Steam              |
|                       | 750 °C (120 min)                               | 1020 °C (60 min) | 1100 °C (60 min) | 1020 °C (3×20 min) |
| Zr1Nb without coating | 6  | 36               | 128              | 45                 |
| Cr/CrN/TiAlN          | $\leq 1$                                       | $\sim 2$         | 12               | $\geq 100$         |
| Cr/CrN/TiAlYn         | $\leq 1$                                       | $\sim 1$         | $\sim 3$         | $\geq 30$          |
| Cr/CrN/TiAlSiN        | $\leq 1$                                       | $\sim 1$         | $\sim 3$         | $\sim 100$         |
| Cr/CrN/TiAlCrYn       | $\leq 1$                                       | $\sim 1$         | $\sim 3$         | $\sim 40$          |
| Cr/TiAlCrY            | $\sim 1$                                       | $\sim 3$         | $\sim 4$         | $\sim 9$           |
| Cr/SS                 | $\sim 2$                                       | $\sim 3$         | $\sim 5$         | $\sim 9$           |
| Cr                    | $\leq 1$                                       | $\sim 2$         | $\sim 3$         | $\sim 3$           |

Regardless of the elemental composition, the only crystalline phase in the surface layer of the coatings is a solid solution based on cubic nitride with a crystal lattice of the NaCl type (structural type B1), which is characteristic of TiN. On the diffractograms, dashed lines show the positions of the diffraction lines of TiN with a crystal lattice period of 0.424 nm. On the diffractograms of Cr/CrN/TiAlN, Cr/CrN/TiAlYn, and Cr/CrN/TiAlCrYn coatings in their original state (see Figs. 3,a; 4,a, and 5,a), the reflections of the solid solution are quite narrow and intense. The size of the crystallites is 20...25 nm. A significant increase in the intensity of the (111) line compared to other reflections of this phase is due to the formation of a strong axial-type texture in the coatings with the [111] axis in the direction normal to the surface. The period of the crystal lattice is 0.419 nm, which is slightly higher than the value calculated according to Vegard's law, and is due to the presence of compressive residual stresses in the coatings. Such a nanocrystalline structure is characteristic of multi-component coatings based on TiN with additives of Al, Cr and Y [14–16, 30–33]. The texture in the coatings is determined by the energy of the ions forming the coating and the homologous temperature [34].

the spinodal decomposition of the metastable supersaturated solid substitution solution, which is characteristic of similar systems [12]. On the diffractogram of the sample with Cr/CrN/TiAlSiN coating (see Fig. 6,a), the nitride lines are much weaker and wider than those of other nitride coatings. The strongest line is (220). The size of the crystallites is only 9 nm. The structure of the coating can be characterized as amorphous-crystalline with the predominant orientation of the nitride crystallites in planes (hh0) parallel to the surface. In this case, the nitride lines are already bifurcated in the initial state. It is known that under certain conditions, the addition of silicon stimulates the disintegration of the solid solution already in the process of coating deposition [14]. Like other diffractograms of coatings, the existing lines weaken after annealing (see Fig. 6,b).

On the diffractograms of the samples with Cr/SS and Cr/TiAlCrY metal coatings (see Figs. 7 and 8, respectively), there are no lines of the Cr sublayer and the substrate, which is due to their greater thickness and density compared to nitride coatings. A cathode made of the corrosion-resistant steel Cr18Ni10T with a high chromium and nickel content was used for the deposition of the Cr/SS coating. This steel belongs to the austenitic class and, after slow cooling, usually has the following structure: austenite (solid solution of carbon and other impurities in  $\gamma$ -Fe), ferrite (solid solution in  $\alpha$ -Fe), and chromium carbide of the  $M_{23}C_6$  type. In the diffractogram of the sample in the initial state only lines of  $\alpha$ -Fe phase are present (see Fig. 7,a), which is most likely due to the non-equilibrium conditions under which deposition occurs and the reduced (compared to the cathode) content of impurities in the coating. The  $\alpha$ -Fe lines are quite intense and narrow, indicating a well-formed crystal structure. The crystallite size of  $\alpha$ -Fe is 60 nm. After oxidation (see Fig. 7,b), the intensity of the  $\alpha$ -Fe lines decreases slightly, and several weak lines appear, which belong to austenite and carbide. At the same time, no oxides are detected and the  $\alpha$ -Fe crystalline phase remains the main phase in the coating.

The diffraction curve of the sample with metal Cr/TiAlCrY coating in the initial state has a halo in the small-angle region and several weak and broad lines (see Fig. 8,a). The structure of the TiAlCrY coating can be characterized as amorphous-crystalline with nanoscale (6...7 nm) particles based on the following phases:  $\alpha$ -Ti with a hcp crystal lattice,  $\text{Cr}_2\text{Ti}$  with a fcc structure, and Cr with a bcc structure.

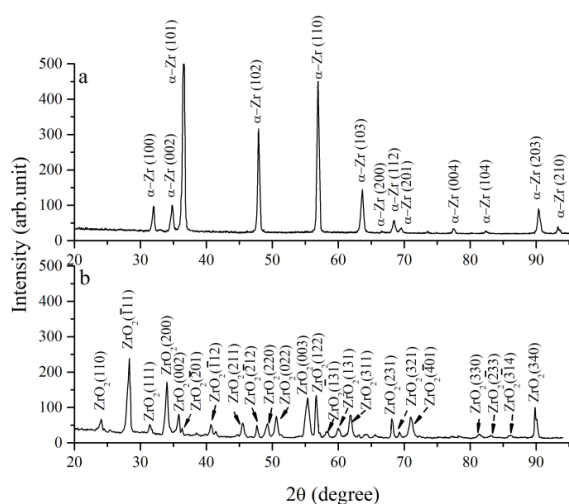


Fig. 2. Diffractograms of uncoated zirconium alloy Zr1Nb in the initial state (a) and after oxidation (b)

After annealing the samples with nitride coatings (see Figs. 3,b; 4,b, and 5,b), the lines on the diffractograms weaken, but no new phases are detected. It should be noted that the intense lines of the nitride bifurcate after annealing, which is most likely caused by

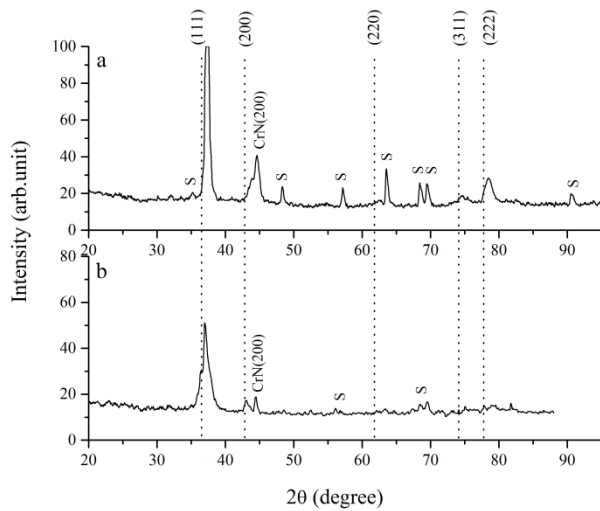


Fig. 3. Cr/CrN/TiAlN coating

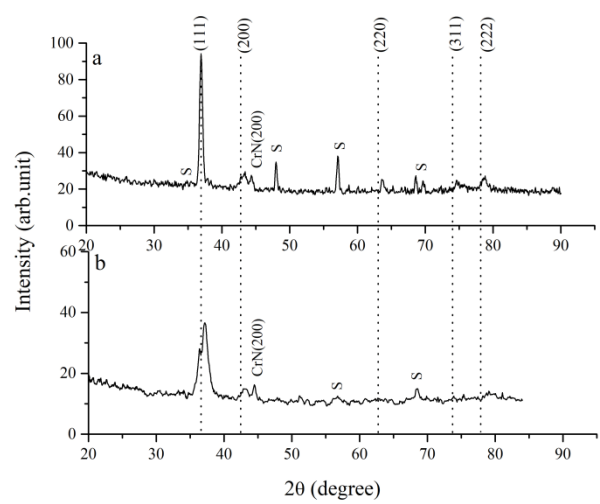


Fig. 4. Cr/CrN/TiAlYN coating

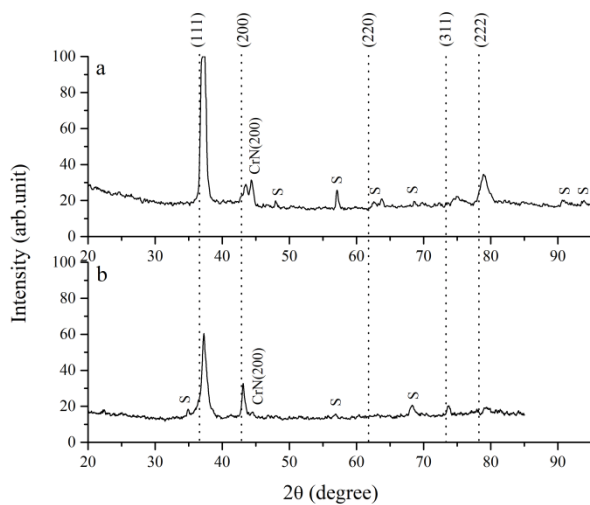


Fig. 5. Cr/CrN/TiAlCrYN coating

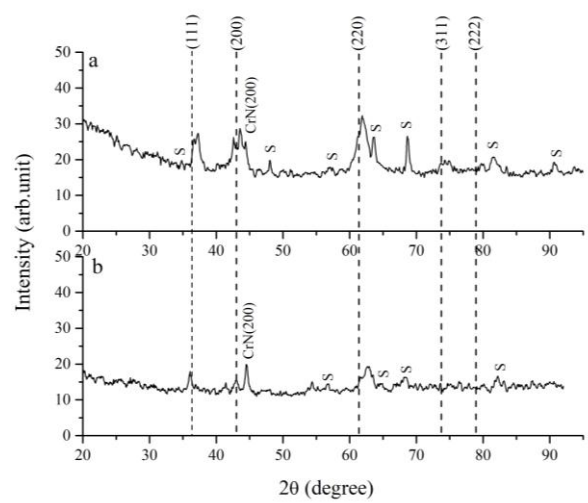


Fig. 6. Cr/CrN/TiAlSiN coating

Figs. 3–6. Diffractograms of samples with nitride coatings in the initial state (a) and after oxidation (b) (S – substrate lines; dashed lines show the position of TiN lines with a cubic lattice of NaCl type)

After oxidation, the amorphous-crystalline structure in the coating is preserved, and no new crystalline phases are detected (see Fig. 8, b).

Thus, the diffractograms of multicomponent coatings are characterized by a weakening of the overall

intensity of the diffraction pattern after oxidation, which is associated with the formation of passivation amorphous oxide layers on the surface of the coatings, which absorb X-ray radiation.

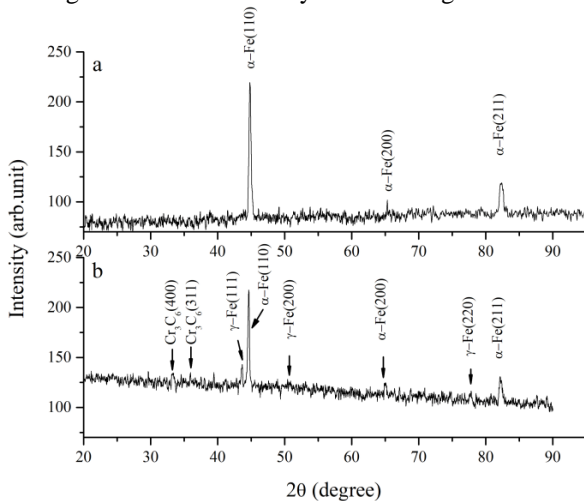


Fig. 7. Diffractograms of the sample with Cr/SS coating in the initial state (a) and after oxidation (b)

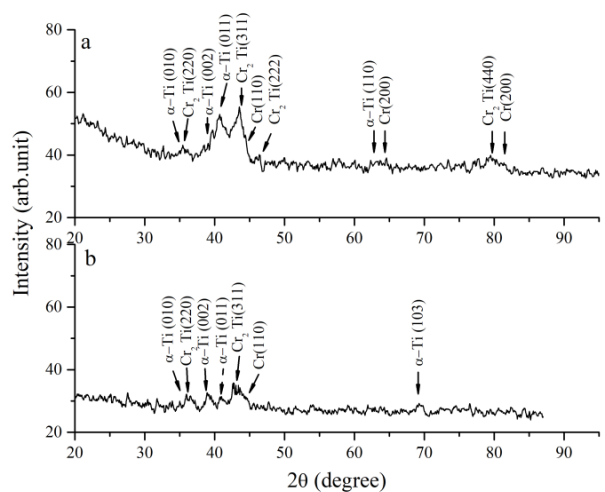


Fig. 8. Diffractograms of the sample with Cr/TiAlCrY coating in the initial state (a) and after oxidation (b)



In the Zr1Nb sample with Cr coating in the initial state, a single phase was detected – Cr with bcc structure. This is the only coating on the surface of which, during high-temperature annealing in air at 1100 °C crystalline oxide is formed. The content of crystalline Cr<sub>2</sub>O<sub>3</sub> in the coating reaches 40 wt.% [23].

Thus, all applied coatings demonstrate sufficiently high stability during tests and can be used to protect zirconium from high-temperature oxidation. When annealing at temperatures up to 1100 °C, the coatings oxidize much more slowly than zirconium alloy. During the test, the coating is not completely oxidized. Oxygen penetrates the surface layer, forming a passivating oxide film, and the phase composition of the subsurface layer does not change significantly.

Protection of the Zr1Nb surface by coatings during thermocyclic oxidation in water steam is less effective than during annealing in air. Thermocycling tests have shown that metal coatings are significantly more efficient than nitride-based coatings. After thermal cycling testing in steam at a temperature of 1020 °C, gray and white oxide precipitates are visible on the uncoated sample. The color of all samples with nitride coating became white and cracks are visible, while on samples with metal coating the surface color is dark and there are no cracks (see Tables 2, 3).

The corrosion kinetics of samples with coatings in steam is shown in Fig. 1,b, and the depth of oxygen penetration in Table 4. The best protection is provided by the Cr coating. The application of Cr reduces the weight gain of the uncoated sample with Zr1Nb by 2.5 times, and the depth of the oxidized layer decreases from 45 to 3 μm. In samples with metal coatings Cr/SS and Cr/TiAlCrY, oxygen penetrates three times deeper, but they prevent oxidation of the zirconium alloy.

On the contrary, nitride coatings cannot withstand the load with an increase in the number of thermal shocks. All the nitride coatings were cracked. Although the coatings were not completely oxidized an oxide layer had formed underneath. The depth of oxygen penetration on samples ranges from 30 to 100 μm. These coatings crack under the influence of thermal shock. Simply holding the coated samples in steam does not lead to cracking. In nitride coatings, the thickness of the oxide layer in this test is an order of magnitude greater than when oxidized in air at the same temperature.

The sharp difference in the behavior of nitride and metal coatings during thermal cycling is because nitride coatings with high internal stresses and low plasticity form cracks [35]. Nitride coatings no longer act as a barrier to oxygen penetration, but rather prevent the formation of a protective layer of zirconium oxide. The Cr/CrN transition sublayer for TiAlN-based coatings is not effective in preventing cracking. The use of hard nitride coatings to protect the Zr1Nb alloy requires the development of damping layers of a different composition.

## CONCLUSIONS

1. NSC KIPT has developed processes for vacuum arc deposition of multi-component coatings based on Cr, Ti, Al, Fe, Y, Si, and their nitrides to protect the

shells of Zr-1Nb alloy fuel rods. The applied deposition processes ensure the formation of coatings with a thickness of 5...9 μm on the cylindrical surface of fuel rod tubes, which have a homogeneous, dense structure and high adhesion to the substrate. Research samples of metallic coatings (Cr, TiAlCrY, FeCrNi) and nitride coatings (TiAlN, TiAlYN, TiAlSiN, TiAlCrYN) were synthesized. The metal coatings have a thin Cr sublayer, and the nitride coatings have a double Cr/CrN sublayer to improve adhesion. The composition, structure, mechanical properties, and resistance to high-temperature oxidation of the samples were studied.

2. Coating leads to hardening of the surface of the Zr1Nb alloy. According to the results of nanoindentation, the hardness of metal coatings is 3...5 GPa, and nitride coatings reach 32...45 GPa.

3. All of the coated fuel cladding samples have better resistance to high-temperature oxidation in air than the Zr1Nb alloy. They oxidize significantly less than uncoated samples at all test temperatures of 750...1100 °C, and this advantage increases with increasing temperature. At an annealing temperature of 1100 °C, the uncoated sample oxidizes to a depth of 130 μm within an hour to form crystalline ZrO<sub>2</sub> oxide, while in the coated samples oxygen penetrates only the surface layer, forming a thin oxide film that prevents further oxidation. The depth of oxygen penetration does not exceed 3...5 μm. The phase composition of the subsurface layer of the coating does not change significantly.

4. The use of coatings to protect Zr1Nb alloy surface against thermal cycling oxidation in water steam is less effective. Thermal cycling tests at a temperature of 1020 °C with three thermal shocks of 20 min each showed that metal coatings are more resistant than nitride-based coatings. The Cr coating oxidizes only up to 3 μm. In the metal coatings Cr/SS and Cr/TiAlCrY, oxygen penetrates three times deeper, but they prevent the oxidation of the zirconium alloy. On the contrary, in the nitride coatings formed cracks and oxygen penetrates under them. The thickness of the oxidized layer in samples with nitride coatings ranges from 30 to 100 μm, while in the Zr1Nb sample without coating, it is about 45 μm.

5. Chrome-based metal coatings demonstrated the best protective properties in tests under simulated accident conditions. They are simultaneously resistant to high-temperature corrosion in air and in water steam during thermal cycling. The use of hard nitride coatings, which significantly strengthen the surface of the zirconium alloy, requires the use of metal damping layers, the optimal thickness and composition of which is yet to be investigated.

## REFERENCES

1. S.J. Zinkle, K.A. Terrani, J.C. Gehin, L.J. Ott, L.L. Snead. Accident tolerant fuels for LWRs: a perspective // *J. Nucl. Mater.* 2014, v. 448, issue 1, p. 374-379.
2. K. Terrani. Accident tolerant fuel cladding development: Promise, status, and challenges // *Journal of Nuclear Materials.* 2018, v. 501, p. 13-30.

3. R.B. Rebak. Innovative accident tolerant nuclear fuel materials will help extending the life of light water reactors // *KOM – Corrosion and Material Protection Journal*. 2022, v. 66, p. 36-39.
4. J. Yanga, M. Steinbrück, C. Tang, M. Große, J. Liua, J. Zhanga, D. Yuna, S. Wang. Review on chromium coated zirconium alloy accident tolerant fuel cladding // *J. Alloys Comp.* 2022, v. 895, p. 162450.
5. Nuclear Engineering International / <https://www.neimagazine.com/news/newswestinghouse-and-edf-co-operate-on-accident-tolerant-fuel-9883963>
6. J. Bischoff, C. Delafoy, C. Vauglin, P. Barberis, C. Roubeyrie, D. Perche, D. Duthoo, F. Schuster, J.-C. Brachet, E.W. Schweitzer, K. Nimishakavi. AREVA NP's enhanced accident-tolerant fuel developments: Focus on Cr-coated M5 cladding // *Nuclear Engineering and Technology*. 2018, v. 50 (2), p. 223-228.
7. A. Fazi, P. Lokhande, D.A. Lopes, K. Stiller, H.-O. Andrén, M. Thuvander. Comparing CrN and TiN Coatings for Accident-Tolerant Fuels in PWR and BWR Autoclaves // *J. Nucl. Eng.* 2022, v. 3, p. 321-332.
8. A. Fazi, H. Aboufadi, A.H.S. Iyer, M. Sattari, K.M. Stiller, P. Lokhande, M. Thuvander, H.O. Andrén. Characterization of as-deposited cold sprayed Cr-coating on Optimized ZIRLO™ claddings // *J. Nucl. Mater.* 2021, v. 549, p. 152892.
9. A. Fazi, K.M. Stiller, H.O. Andrén, M. Thuvander. Cold sprayed Cr-coating on Optimized ZIRLO™ claddings: the Cr/Zr interface and its microstructural and chemical evolution after autoclave corrosion testing // *J. Nucl. Mater.* 2022, v. 560, p. 153505.
10. A. Fazi, M. Sattari, K. Stiller, H.-O. Andrén, M. Thuvander. Performance and evolution of cold spray Cr-coated optimized ZIRLO™ claddings under simulated loss-of-coolant accident conditions // *J. Nucl. Mater.* 2023, v. 576, p. 154268.
11. S. Veprek, P. Holubar, M. Veprek-Heijman. Industrial Applications of Hard and Superhard Nanocomposite Coatings on Tools for Machining, Forming, Stamping and Injection Molding // *Advanced Materials Research*. 2016, v. 1135, p. 218-233.
12. S. Veprek, M. Veprek-Heijman, P. Karvankova, J. Prochazka. Different approaches to superhard coatings and nanocomposites // *Thin Solid Films*. 2005, v. 476, p. 1-29.
13. E.N. Reshetnyak, V.E. Strel'nitskij. Synthesis of hardening nanostructural coatings // *Problems of Atomic Science and Technology*. 2008, N 2, p. 119-130.
14. V.A. Belous, A.S. Kuprin, S.N. Dub, V.D. Ovcharenko, G.N. Tolmacheva, E.N. Reshetnyak, I.I. Timofeeva, P.M. Litvin. Structure and mechanical properties of Ti-Al-Si-N protective coatings deposited from separated plasma of a vacuum Arc // *Journal of Superhard Materials*. 2013, v. 35(1), p. 20-28.
15. V.A. Belous, V.V. Vasylyev, V.S. Goltvyanytsya, S.K. Goltvyanytsya, A.A. Luchaninov, E.N. Reshetnyak, V.E. Strel'nitskij, G.N. Tolmacheva, O. Danylina. Structure and properties of Ti-Al-Y-N coatings deposited from filtered vacuum-arc plasma // *Surface & Coatings Technology*. 2011, v. 206, p. 1720-1726.
16. V.V. Vasylyev, V.S. Goltvyanytsya, S.K. Goltvyanytsya, A.A. Luchaninov, V.G. Marinin, E.N. Reshetnyak, V.E. Strel'nitskij, G.N. Tolmacheva. Durability of the multicomponent nitride coatings based on TiN and (Ti,Al)N deposited by PIII&D method // *Problems of Atomic Science and Technology*. 2015, N 2, p. 130-138.
17. P.P. Joshi, N. Kumar, K.L. Murty. *Materials for Nuclear Reactors: Encyclopedia of Materials: Metals and Alloys*. Elsevier Inc., 2022, v. 1, p. 364-376.
18. E. Alat, A.T. Motta, R.J. Comstock, J.M. Parvezana, D.E. Wolfe. Ceramic coating for corrosion (c3) resistance of nuclear fuel cladding // *Surface and Coatings Technology*. 2015, v. 281, p. 133-143.
19. E. Alat, A.T. Motta, R.J. Comstock, J.M. Parvezana, D.E. Wolfe. Multilayer (TiN, TiAlN) ceramic coatings for nuclear fuel cladding // *Journal of Nuclear Materials*. 2016, v. 478, p. 236-244.
20. M.J. Brova, E. Alata, M.A. Pauleya, R. Sherbondy, A.T. Motta, D.E. Wolfe. Undoped and ytterbium-doped titanium aluminum nitride coatings for improved oxidation behavior of nuclear fuel cladding // *Surface and Coatings Technology*. 2017, v. 331, p. 163-171.
21. V.A. Belous, S.A. Leonov, G.I. Nosov, V.M. Khoroshikh, N.S. Lomino, G.N. Tolmacheva, M.A. Brovina, I.G. Yermolenko. Modification of the surface of alloy E110 by sedimentation multilayered Zr/ZrN coverings and ionic irradiation // *PSE*. 2009, v. 7, N 1-2, p. 76-81.
22. A. Kuprin, V. Belous, V. Voyevodin, V. Bryk, R. Vasilenko, V. Ovcharenko, E. Reshetnyak, G. Tolmacheva, P. V'yugov. Vacuum-arc chromium-based coatings for protection of zirconium alloys from the high-temperature oxidation in air // *J. Nucl. Mater.* 2015, v. 465, p. 400-406.
23. A.S. Kuprin, V.A. Belous, V.V. Bryk, R.L. Vasilenko, V.N. Voyevodin, V.D. Ovcharenko, G.N. Tolmacheva, I.V. Kolodiy, V.M. Lunyov, I.O. Klimenko. Vacuum-arc chromium coatings for Zr-1Nb alloy protection against high-temperature oxidation in air // *Problems of Atomic Science and Technology*. 2015, N 2(96), p.111-118.
24. V.A. Belous, P.N. V'yugov, A.S. Kuprin, G.N. Tolmacheva, V.M. Khoroshikh. Mechanical characteristics of Zr1Nb alloy tube after deposition of ion-plasma coatings // *Problems of Atomic Science and Technology*. 2013, N 2, p.140-143.
25. A.S. Kuprin, V.A. Belous, V.N. Voyevodin, G.N. Tolmacheva, P.N. V'yugov. High-temperature air oxidation of E110 and Zr-1Nb alloys claddings with coatings // *Problems of Atomic Science and Technology*. 2014, N 1(89), p. 126-132.
26. R.L. Vasilenko, V.N. Voyevodin, V.A. Belous, M.A. Bortnitskaya, I.V. Kolodiy, I.O. Klimenko, V.D. Ovcharenko, V.I. Kovalenko, V.G. Marinin, A.V. Ilchenko, M.A. Tikhonovsky, A.S. Kuprin. Structure and properties of FeCr, CrAl and FeCrAl coatings deposited by cathodic arc evaporation // *Problems of Atomic Science and Technology*. 2021, N 2(132), p. 119-128.

27. Raul B. Rebak. Accident Tolerant Materials for Light Water Reactor Fuels. Elsevier, 2020; <https://doi.org/10.1016/C2018-0-02102-7>.
28. V.A. Belous, V.N. Voyevodin, V.M. Khoro-shikh, A.S. Kuprin, L.O. Shpagina. Prototype equipment and techniques for obtaining cavitation-resistant coatings to be applied to working surfaces of steam turbine blades made of VT6 titanium alloy in order to replace imported counterparts // *Science and Innovation*. 2016, v. 12(4), p. 27-35.
29. W.C. Oliver, G.M. Pharr. Measurement of hardness and elastic modulus by instrumented indentation: Advances in understanding and refinements to methodology // *Journal of Materials Research*. 2004, v. 19 (1), p. 3-20.
30. V.V. Vasiliev, A.A. Luchaninov, E.N. Reshetnyak, V.E. Strel'nitskij, G.N. Tolmacheva, M.V. Reshetnyak. Structure and hardness of Ti-N and Ti-Si-N coatings deposited from filtered vacuum-arc plasma // *Problems of Atomic Science and Technology*. 2009, N 2, p. 173-180.
31. V.A. Belous V.V. Vasiliev, A.A. Luchaninov, E.N. Reshetnyak, V.E. Strel'nitskij, G.N. Tolmacheva, V.S. Goltvyanitsa, S.K. Goltvyanitsa. Ti-Al-N hard coatings deposited from filtered vacuum-arc plasma // *Physical surface engineering*. 2009, v.7, N 3, p. 216-222.
32. E. Reshetnyak. Structure and stress state of TiN and  $Ti_{0.5-x}Al_{0.5}Y_xN$  coatings prepared by the PIII&D technique from filtered vacuum-arc plasma // *Problems of Atomic Science and Technology*. 2014, N 1, p. 159-162.
33. L.I. Gladkikh, S.V. Malykhin, A.T. Pugachov, E.N. Reshetnyak, D.B. Glushkova, S.S. Dyachenko, G.P. Kovtun. Residual stresses and structure of coatings of titanium and chromium nitrides obtained by ion-plasma deposition // *Metallophysics and Advanced Technologies*. 2003, v. 25, N 6, p. 763-776.
34. A. Kalinichenko, E. Reshetnyak, V. Strel'nitskij, G. Abadias. Role of nonlocal thermoelastic peaks in the stress and texture evolution of TiN coatings formed by plasma based ion implantation and deposition // *Surface & Coatings Technology*. 2020, v. 391, p. 125695.
35. Y. Liu, I. Bhamji, P.J. Withers, D.E. Wolfe, A.T. Motta, M. Preuss. Evaluation of the interfacial shear strength and residual stress of TiAlN coating on ZIRLO™ fuel cladding using a modified shear-lag model approach // *Journal of Nuclear Materials*. 2015, v. 466, p. 718-727.

Article received 28.02.2023

## **ЗАХИСНІ ВАКУУМНО-ДУГОВІ ПОКРИТТЯ НА ПАЛИВНИХ ОБОЛОНКАХ З ЦИРКОНІЄВИХ СПЛАВІВ ДЛЯ ЗАПОБІГАННЯ КАТАСТРОФІЧНОМУ РОЗВИТКУ АВАРІЙНИХ СИТУАЦІЙ НА ЯДЕРНИХ РЕАКТОРАХ**

*О.С. Купрін, В.А. Зуйок, В.А. Білоус, В.Д. Овчаренко, О.М. Решетняк, Р.Л. Василенко,  
Г.М. Толмачова, Я.О. Куштим*

Розроблено процеси вакуумно-дугового осадження багатокомпонентних покриттів на основі Cr, Ti, Al, Fe, Y, Si та їх нітридів товщиною 5...9 мкм для захисту оболонок палива з цирконієвих сплавів. Склад, структуру та механічні властивості покриттів визначено методами електронної мікроскопії, енергодисперсійної рентгенівської спектроскопії, рентгеноструктурного аналізу та наноіндентування. Проведено порівняльні дослідження захисних властивостей покриттів при високотемпературному окисленні труб Zr1Nb. Було виявлено, що металеві покриття з високим вмістом хрому мають високі захисні властивості під час випробувань в імітованих умовах аварії. Вони одночасно стійкі до високотемпературної корозії на повітрі при температурі 750...1100 °C і у водяній парі при термоцикуванні до 1020 °C. Тверді нітридні покриття, які значно зміцнюють поверхню цирконієвого сплаву і добре захищають від окислення на повітрі, менш ефективні в парах води при термоцикуванні. Розроблені у ННЦ ХФТІ покриття та процеси синтезу можуть бути корисні при вдосконаленні топливних оболонок із сплавів цирконію провідного світового виробника ядерного палива Westinghouse Electric Company.